International Journal of Electrical and Electronics Engineering (IJEEE)
ISSN 2278-9944
Vol. 2, Issue 4, Sep 2013, 9-20

International Academy of Science, Engineering and Technology
Connecting Researchers; Nurturing Innovations

TE AND TM MODAL DISPERSION IN CYLINDRICAL LOSSY TERAHERTZ METAMATERIAL WAVEGUIDE

HASSAN S. ASHOUR

Department of Physics, Al-Azhar University, Gaza, Palestine

Department of Physics, University of Dayton, Dayton, Ohio, USA

ABSTRACT

In this work, we derive the TE and TM modal dispersion relation for a cylindrical waveguide with dielectric core and two classes of Terahertz left-handed material were used. The first class uses 3D nano-spheres distributed in loops in the dielectric host material, which gives rise to negative effective permeability and permeability at Terahertz (optical) frequencies. The second class is the nanorods that result in negative effective permeability and permeability at optical frequencies used in communications. We numerically solved the modal dispersion relation, and the power confinement for Terahertz TE and TM modes for a given set of parameters including operating frequency, core's radii, and power confinement factor and extinction coefficient. We found that the real and imaginary (extinction coefficient) parts of the effective refractive index exhibit small values. Besides that, the power confinement in the dielectric core increased as core's radius increased and the power attenuation deceased as core's radius increased.

KEYWORDS: Cylindrical Waveguide, Dispersion Relation, Left Handed Material LHM Surface Waves, Power Confinement

INTRODUCTION

In 1968, Veselago had proposed a peculiar class of material [1], which exhibits negative permeability and negative permittivity. He called this class of materials by left handed material, or sometimes called double negativity material DNM. In 2001, a group of researchers were able to synthesize an artificial dielectric medium (Metamaterials). They were able to demonstrate that those materials exhibit both negative dielectric permittivity and magnetic permeability simultaneously over a certain range of frequencies [2]. Since then, left hand materials (LHM) had grabbed the attention of many researchers in many scientific communities, because of its bazaar characteristics and wide promise of unusual applications. Nowadays, Metamaterials are used in fabricating Transmission Lines [3, 5], Microstrip Resonators [6], Couplers [7, 8], Resonators [9], Wave Division Multiplexors (WDM) [10],and Antennas [11]. However, many applications demands a class of Metamaterials that operates at optical frequencies, i.e. integrated metamaterial modulator on optical fiber [12, 13], which was the driving force to realize such Metamaterials that operate at optical frequencies [14-20]. This wide spectrum of applications motivated us to investigate the propagation of $TE$and TM mode in a cylindrical structure with dielectric core material and cladding made of a Terahertz left handed material. This paper is organized as follows: 2 we derive the TE and TM modal dispersion relation for a cylindrical waveguide with dielectric core and Terahertz left-handed material cladding; 3 we discuss the numerical results 4 is solely devoted to the conclusion.

THEORY

Dispersion Relations

Here, we briefly outline the derivation of the dispersion relations [21-24] for TE, and TM in a cylindrical waveguide structure with dielectric core of radius a, index $n_1 = \sqrt{\varepsilon_r(\omega)}$ and a Terahertz left-handed material cladding of

index $n_2 = \sqrt{\varepsilon_{r(eff)}(\omega)}$. In general, the electromagnetic fields in optical fibers are expressed in cylindrical coordinates as follow

$$\tilde{E} = E(r,\theta)\mathrm{e}^{i(\omega t - \beta z)} \tag{1}$$

$$\tilde{H} = H(r,\theta)\mathrm{e}^{i(\omega t - \beta z)} \tag{2}$$

Where ω is the applied angular frequency, $z - axis$ indicates the propagation direction, and β is the complex effective wave index and is given by

$$\beta = n - i\gamma \tag{3}$$

Where n is the real part of the effective wave index (effective refractive index of the structure), and γ is called the extinction coefficient or the absorption coefficient. Substituting equations (1) and (2) in the Maxwell equation in the cylindrical coordinates will result in electric field components,

$$\frac{1}{r}\frac{\partial E_z}{\partial \theta} + i\beta E_\theta = -i\omega\mu H_r \tag{4.1}$$

$$\frac{\partial E_z}{\partial r} + i\beta E_r = -i\omega\mu H_\theta \tag{4.2}$$

$$\frac{1}{r}\frac{\partial (rE_\theta)}{\partial r} - \frac{1}{r}\frac{\partial E_r}{\partial \theta} = -i\omega\mu H_z \tag{4.3}$$

and the follwoing set equations for the magnetic field components,

$$\frac{1}{r}\frac{\partial H_z}{\partial \theta} + i\beta H_\theta = i\omega\varepsilon E_r \tag{5.1}$$

$$\frac{\partial H_z}{\partial r} + i\beta H_r = -i\omega\varepsilon E_\theta \tag{5.2}$$

$$\frac{1}{r}\frac{\partial (rH_\theta)}{\partial r} - \frac{1}{r}\frac{\partial H_r}{\partial \theta} = i\omega\varepsilon E_z \tag{5.3}$$

From equations 4 and 5, we can write the scalar wave equations for the electric and magnetic field components in the waveguide as,

$$\frac{\partial^2 E_z}{\partial r^2} + \frac{1}{r}\frac{\partial E_z}{\partial r} + \frac{1}{r}\frac{\partial^2 E_z}{\partial \theta^2} + [\omega^2\mu(\omega)\varepsilon(\omega) - \beta^2]E_z = 0 \tag{6}$$

$$\frac{\partial^2 H_z}{\partial r^2} + \frac{1}{r}\frac{\partial H_z}{\partial r} + \frac{1}{r}\frac{\partial^2 H_z}{\partial \theta^2} + [\omega^2\mu(\omega)\varepsilon(\omega) - \beta^2]H_z = 0 \tag{7}$$

Using equations 4 and 5 to rewrite equations 6 and 7 in terms of the axial field components E_z, H_z gives,

$$\frac{\partial^2 E_z}{\partial r^2} + \frac{1}{r}\frac{\partial E_z}{\partial r} + \frac{1}{r^2}\frac{\partial^2 E_z}{\partial \theta^2} + [\omega^2\mu(\omega)\varepsilon(\omega) - \beta^2]E_z = 0 \tag{8}$$

$$\frac{\partial^2 H_z}{\partial r^2} + \frac{1}{r}\frac{\partial H_z}{\partial r} + \frac{1}{r^2}\frac{\partial^2 H_z}{\partial \theta^2} + [\omega^2\mu(\omega)\varepsilon(\omega) - \beta^2]H_z = 0 \tag{9}$$

Since we are dealing with circularly symmetric structure, we anticipate periodic solution in the angular coordinate θhave the following form,

$$\psi(r,\theta) = R(r)e^{iv\theta} \tag{10}$$

Where $\psi(r,\theta)$ is either E_z or H_z and $v = 0,1,2,3,\ldots$. Substituting equation10 in equations 8 and 9, we arrive at the scalar wave equation for circular waveguide

$$\frac{\partial^2 R}{\partial r^2}+\frac{1}{r}\frac{\partial R}{\partial r}+\left[k^2n^2-\beta^2-\frac{v^2}{r^2}\right]R=0 \tag{11}$$

These are the well-known Bessel differential equations, which can be solved for the electric fields and magnetic fields in the core

$$\frac{\partial^2 R}{\partial r^2}+\frac{1}{r}\frac{\partial R}{\partial r}+\left[\frac{u^2}{a^2}-\frac{v^2}{r^2}\right]R=0 \tag{12}$$

and for the cladding

$$\frac{\partial^2 R}{\partial r^2}+\frac{1}{r}\frac{\partial R}{\partial r}-\left[\frac{w^2}{a^2}+\frac{v^2}{r^2}\right]R=0 \tag{13}$$

Where$u^2=a^2[\omega^2\mu_c(\omega)\varepsilon_c(\omega)-\beta^2]$, $w^2=a^2[\beta^2-\omega^2\mu_{cl}(\omega)\varepsilon_{cl}(\omega)]$, $\mu_c(\omega)=\mu_r\mu_0=\mu_0$, $\varepsilon_c(\omega)=\varepsilon_0\varepsilon_r(\omega)$ are the core's permeability and permittivity, $\mu_{cl}(\omega)=\mu_0\,\mu_{eff}(\omega)$ and $\varepsilon_c(\omega)=\varepsilon_0\varepsilon_{eff}(\omega)$are the left-handed material cladding's permeability and permittivity.The general solutions of equations 12 and 13 are the following

$$E_z=\frac{AJ_v\left(\frac{u}{a}r\right)}{J_v(u)},r\le a \tag{14.1}$$

$$E_z=\frac{AK_v\left(\frac{w}{a}r\right)}{K_v(u)},r>a \tag{14.2}$$

and

$$H_z=\frac{BJ_v\left(\frac{u}{a}r\right)}{J_v(u)},r\le a \tag{15.1}$$

$$H_z=\frac{BK_v\left(\frac{w}{a}r\right)}{K_v(u)},r>a \tag{15.2}$$

Where A and B are constants. Using equation 14 in equations 4 and 5, the field components are

$$E_r=-\frac{a^2}{u^2}\left(\frac{v\omega\mu_0 BJ_v\left(\frac{ur}{a}\right)}{rJ_v(u)}-\frac{i\beta Au\,J_v'\left(\frac{ur}{a}\right)}{aJ_v(u)}\right),r\le a \tag{16.1}$$

$$E_r=\frac{a^2}{w^2}\left(\frac{v\omega\mu_{cl}BK_v\left(\frac{wr}{a}\right)}{rK_v(w)}-\frac{i\beta Au\,K_v'\left(\frac{wr}{a}\right)}{aK_v(w)}\right),r>a \tag{16.2}$$

$$E_\theta=-\frac{a^2}{u^2}\left(\frac{i\omega\mu_0 BuJ_v'\left(\frac{ur}{a}\right)}{aJ_v(u)}+\frac{\beta vAJ_v\left(\frac{ur}{a}\right)}{rJ_v(u)}\right),r\le a \tag{17.1}$$

$$E_\theta=\frac{a^2}{w^2}\left(\frac{i\omega\mu_{cl}BwK_v'\left(\frac{wr}{a}\right)}{aK_v(w)}+\frac{\beta vAK_v\left(\frac{wr}{a}\right)}{rK_v(w)}\right),r>a \tag{17.2}$$

The magnetic field has a similar set, which has the following form

$$H_r=\frac{a^2}{u^2}\left(\frac{v\varepsilon_c(\omega)\omega AJ_v\left(\frac{ur}{a}\right)}{rJ_v(u)}+\frac{i\beta Bu\,J_v'\left(\frac{ur}{a}\right)}{aJ_v(u)}\right),r\le a \tag{18.1}$$

$$H_r=-\frac{a^2}{w^2}\left(\frac{v\varepsilon_{cl}(\omega)A\omega K_v\left(\frac{wr}{a}\right)}{rK_v(w)}+\frac{i\beta Bw\,K_v'\left(\frac{wr}{a}\right)}{aK_v(w)}\right),r>a \tag{18.2}$$

$$H_\theta=\frac{a^2}{u^2}\left(\frac{i\varepsilon_c(\omega)\omega Au\,J_v'\left(\frac{ur}{a}\right)}{aJ_v(u)}-\frac{\beta vBJ_v\left(\frac{ur}{a}\right)}{rJ_v(u)}\right),r\le a \tag{19.1}$$

$$E_\theta = -\frac{a^2}{w^2}\left(\frac{i\omega\varepsilon_{cl}(\omega)\omega A w\, K_v'\left(\frac{wr}{a}\right)}{aK_v(w)} - \frac{\beta v B\, K_v\left(\frac{wr}{a}\right)}{rK_v(w)}\right), r > a \tag{19.2}$$

Applying the boundary conditions at $r = a$ and evaluating the ratio of the constants A and B, we can find the eigenvalue equation. The guided modes dispersion relation can be obtained from equations 16 to 19

$$\left[\frac{J_v'(u)}{uJ_v(u)} + \frac{\mu_{cl}}{\mu_c}\frac{K_v'(w)}{wK_v(w)}\right]\left[\frac{J_v'(u)}{uJ_v(u)} + \frac{\varepsilon_{eff}(\omega)}{\varepsilon_r(\omega)}\frac{K_v'(w)}{wK_v(w)}\right] = \frac{\beta^2 k_0^2 a^4 v^2(\varepsilon_c(\omega)\mu_c(\omega) - \varepsilon_{cl}(\omega)\mu_{cl}(\omega))}{u^4 w^4 \varepsilon_c(\omega)\mu_c(\omega)} \tag{20}$$

The guided modes have one of two possible polarizations for each v. For the special case $v = 0$, the TE and TM polarized modes arise. Thus, the right hand side of equation 20 vanishes. For TE mode ($E_z = 0$) which gives the TE mode dispersion equation we will have

$$\frac{J_v'(u)}{uJ_v(u)} = -\frac{\mu_{cl}}{\mu_c}\frac{K_v'(w)}{wK_v(w)} = -\frac{\mu_0\,\mu_{eff}(\omega)}{\mu_0}\frac{K_v'(w)}{wK_v(w)} = \frac{J_1(u)}{uJ_0(u)} = -\mu_{eff}(\omega)\frac{K_v'(w)}{wK_v(w)} \tag{21}$$

and for TM mode ($H_z = 0$), which gives the TM mode dispersion equation

$$\frac{J_v'(u)}{uJ_v(u)} = -\frac{\varepsilon_{eff}(\omega)}{\varepsilon_r(\omega)}\frac{K_v'(w)}{wK_v(w)} \tag{22}$$

Solving equations 16, would give the magnetic fields for the TE mode

$$H_z(0 \le r \le a) = AJ_0(\kappa r) \tag{23.1}$$

$$H_z(r > a) = BK_0(\sigma r) \tag{23.2}$$

The solution of equation 16 for the electric field for the TM mode

$$E_z = AJ_0(\kappa r),\ \ 0 \le r \le a \tag{24.1}$$

$$E_z = BK_0(\sigma r),\ \ r > a \tag{24.2}$$

The Terahertz left-handed material used in this structure possesses negative frequency dispersion at optical frequencies. The frequency dependence of the cladding dielectric permittivity and magnetic permeability were achieved by inserting a circular array of equi-spaced sliver nano-spheres in a host dielectric material as in figure 1. The new design idea depends on the collective resonance of a circular pattern array of plasmonic nano-particles. In this ring, the plasmonic resonant feature of every nano-particle that induces a circulating "displacement" current around this loop [16]. Unlike the case of the conventional metallic loops or SRRs at the microwave frequencies, but rather the plasmonic resonant frequency of the nano-particle is the main determining factor for this resonance to happen [16].

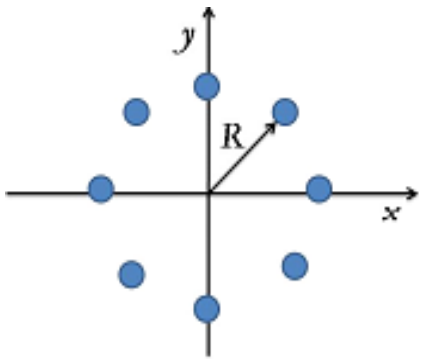

Figure 1: A Circular Array with N = 8 Equi-Spaced Nano-Spheres in the x-y, with Circle's Radius R

$$\mu_{eff}(\omega) = \mu_0\left(1 + \frac{1}{N[\alpha_{mm}^{-1} + i(k_b^3)] - 1/3}\right) \tag{25}$$

where,

$$\alpha_{mm}^{-1} = \frac{4\varepsilon_b}{Nk_b^2R^2}\alpha - i\left(\frac{k_b^3}{6\pi} - \frac{2k_b}{3\pi NR^2}\right) + \frac{1}{16\pi Nk_b^2R^5}\sum_{l\neq n}^{N}\frac{3+\cos^2[2\pi(l-n)/N]}{\sin^2[\pi(l-n)/N]^3} \quad (26)$$

α_{mm} is the magnetic polarizability of the nano-ring, N number of the identical nano-spheres with radius a, λ_b is the wave length in the background medium, R is the circle's radius, $\varepsilon_b$is the background dielectric material constant, $k_b = \omega\sqrt{\varepsilon_b\mu_0}$is the background wave number,$n = 1,2, \ldots N$, and α is given by,

$$\alpha = \left[\left(4\pi\varepsilon_b a^3\frac{\varepsilon-\varepsilon_b}{\varepsilon+2\varepsilon_b}\right)^{-1} - i\frac{k_b^3}{6\pi\varepsilon_b}\right]^{-1} \quad (27)$$

where ε is the permittivity of a single isolated nano-sphere, and the effective permittivity is given by

$$\varepsilon_{eff}(\omega) = \varepsilon_0\left(1 + \frac{1}{\varepsilon_0 N_d^{-1}\left[\alpha_{ee}^{-1} + i\left(k_0^3/_{6\pi\varepsilon}\right)\right]^{-1/3}}\right) \quad (28)$$

where N_d is number density of the loop inclusions per unit volume, α_{ee} is electric polarizability of the loop, and $k_0 = \omega\sqrt{\varepsilon_0\mu_0}$ is the background wave number. Equations 1 through 4 are obtained in the limit $k_b \ll 1$and $a \ll R \ll \lambda_b$. The material exhibited both negative effective permeability and negative permittivity, in the frequency rang $630\,THz$ to $634\,THz$, at optical frequency for the following parameters: $R = 40nm, a = 16nm, N = 6, N_d = (108nm)^{-3}$, and $\varepsilon_b = 2.2\varepsilon_0$. These values would give rise to both effective permittivity and permeability has negative real parts simultaneously in the frequency spectrum $630 - 634\,THz$. The core's dielectric constant $\varepsilon_r(\omega)$for BaF_2can be obtained from Sellmeier dispersion relationship, which is given by [25]

$$\varepsilon(\lambda) = 1 + \frac{A_1\lambda^2}{\lambda^2-\lambda_1^2} + \frac{A_2\lambda^2}{\lambda^2-\lambda_2^2} + \frac{A_3\lambda^2}{\lambda^2-\lambda_3^2} + \cdots \quad (29)$$

where $\lambda_i$is a constant, and $A_1, A_2, A_3, \lambda_1, \lambda_2, \lambda_3$ are called Sellmeier coefficients, and have the following values for BaF_2glass: $A_1 = 0.63356,\ A_2 = 0.506762,\ A_3 = 3.8261,\ \lambda_1 = 0.057789,\ \lambda_2 = 0.109681, and\ \lambda_3 = 46.38642.$

Confinement Factors

The power confinement factor of a waveguide can be obtained by calculating the power flow in the core to the total power flow in the waveguide structure. The time average Poynting vector component along the direction of propagation, z-axis, per unit area is given by

$$S_z = \frac{1}{2}(E \times H^*)\cdot u_z = \frac{1}{2}(E_r H_\theta^* - E_\theta H_r^*) \quad (30)$$

TE Node Confinement Factor

The transmission power in the core and cladding are calculated from equation 16 to 18 and substituted inequations 30, to give

$$P_{core} = \pi\omega\mu_0\beta|A|^2\left(\frac{a}{u}\right)^2\int_0^a J_1^2\left(\frac{u}{a}r\right)dr \quad (31)$$

$$P_{clad} = \pi\omega\mu_0\beta|A|^2\left(\frac{a}{w}\right)^2\frac{J_0^2(u)}{K_0^2(w)}\int_a^\infty K_1^2\left(\frac{w}{a}r\right)dr \quad (32)$$

Integrating over the specified intervals or using Bessel identities, we have the power flow in the core and cladding as

$$P_{core} = \frac{\pi}{2}\omega\mu_0\beta|A|^2\left(\frac{a^2}{u}\right)^2 J_1^2(u)\left[1+\frac{w^2}{u^2}\frac{K_0(w)K_2(w)}{K_1^2(w)}\right] \quad (33)$$

$$P_{clad} = \frac{\pi}{2}\omega\mu_0\beta|A|^2\left(\frac{a^2}{u}\right)^2 J_1^2(u)\left[\frac{K_0(w)K_2(w)}{K_1^2(w)}-1\right] \quad (34)$$

The total power carried by TE mode is given by

$$P = P_{core} + P_{clad} \quad (35)$$

The confinement factor is

$$\Gamma = \frac{P_{core}}{P} = 1-\frac{u^2}{v^2}\left[1-\frac{K_1^2(w)}{K_0(w)K_2(w)}\right] \quad (36)$$

where$v^2 = u^2 + w^2$

TM Mode Confinement Factor

Substituting equations 14and 16 in equation 30, we can find the power flow for TM mode as

$$P_{core} = \frac{\pi}{2}\omega\varepsilon_0\beta|A|^2\left(\frac{a^2}{u}\right)^2 [J_1^2(u)-J_0(u)J_2(u)] \quad (37)$$

$$P_{clad} = \frac{\pi}{2}\omega\varepsilon_0 n_0^2\beta|A|^2\left(\frac{a^2}{w}\right)^2 \frac{J_0^2(u)}{K_0^2(w)}[K_0(w)K_2(w)-K_1^2(w)] \quad (38)$$

$$\Gamma = \frac{P_{core}}{P_{clad}+P_{core}} \quad (39)$$

NUMERICAL RESULTS AND DISCUSSIONS

In this section, we explore the numerical solutions of the dispersion relations for TE and TMmodes, equation 21 and 22, and the power confinement factor for TE and TMmodes, equations 36 and 39. We found the complex effective wave index $\beta = n - i\gamma$ as a function of the electromagnetic wave at Terahertz frequency spectrum between $630\sim 634$ Terahertz, and for practical dielectric core's radii(a $= 4, 8, and\ 16\ \mu m$). The parameters of the Terahertz LHM have been adjusted to have negative effective permittivity and negative effective permeability over the previously mentioned frequency spectrum.

In figure 2, we plotted the real part of the effective refractive index,n, versus the allowed frequency range for different dielectric core's radii, with dielectric constant for BaF_2 glass calculated using equation (29). Figure 2 shows that the real part of the effective refractive index, n, for TE and TM mode for different core's radii. We can notice that the real part of the effective refractive index is almost zero over the specified frequency spectrum for both modes of polarization, which means the phase of the wave front suffers minimum changes upon propagation in this waveguide structure. In figure 2-a, the real part of the effective refractive index for $a = 4\ \mu m$ (solid line curve)increases with frequency increase with positive slope, which means the waveguide behaves like a right handed material. The slope of the dispersion relation represents the group velocity [26, 27]. When the slope has a positive gradient this means that the group velocity is positive, and the structure behaves like RHM (right handed material). This behavior continues with core's radii8 μm (dashed line curve) and $16\ \mu m$ (dotted-dash line curve), but with steeper slope. In figure 3-b, the real part of the effective refractive index of the TM mode claims lower values than the TE mode with small positive slope. In either case, the real part of the effective refractive index is small and can be approximated to zero, which is a common feature of these curves with small variation across the allowed frequency spectrum. This class of structures is important in many applications [28], since the phase variation over the wavefront is very small.

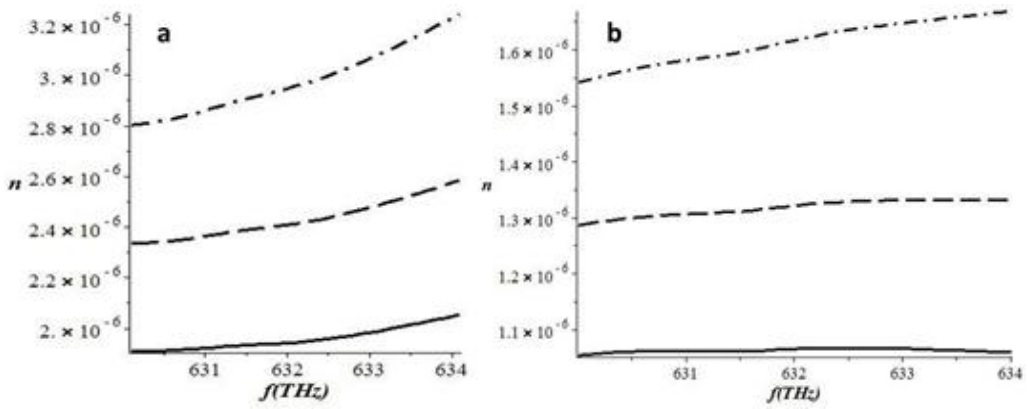

Figure 2: Real Part of the Effective Index for a. TE Mode, and b. TM Mode for Core's Radii a $= 4\mu m$ (Solid), $\mu m8$(Dashed), and $16\mu m$(Dot $-$ Dash) μm

In figure 3, we plot the imaginary part of the effective refractive index, which is called the extinction (or absorption) coefficientγ, of the structure versus the allowed frequency range. It can be noticed that the values of the extinction coefficient are small and decrease with the cores radii increase for both TE and TM modes.

Moreover, small values of the extinction coefficient indicate that the structure is somehow transparent. It is evident from figure 3 a and b, that both TE and TM suffers the same attenuation in this class of cylindrical waveguides. Besides that, the extinction coefficient decreases with frequency increase, and also with core's radii increase.

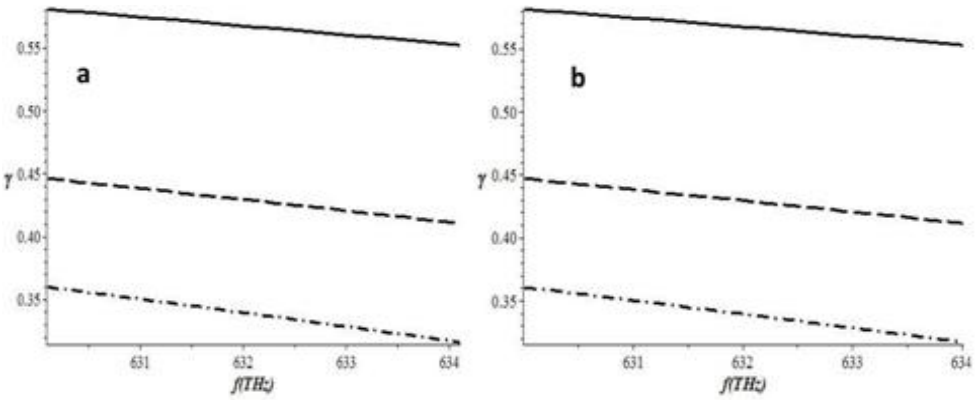

Figure 3: Extinction Coefficient, Imaginary Part of the Effective Index, for a. TE Mode, and b. TM Mode for Core's Radii a $= 4\mu m$ (Solid), $\mu m8$(Dashed), and $16\mu m$(Dot $-$ Dash) μm

In figure 4-a, we plot the power confinement factor for TE modes (equation 36) versus the allowed frequency range for different core's radii. Figure 4-a shows that the power confinement factor has higher values as the core radius increases, thus we have better power confinement for wider cores.

The power confinement factor for TE modespeaks at $f = 632THz$ and then it drops back with frequency increase. This implies the structure guides the optical power through the core more than wasting it in the cladding, with better confinement at $f = 632THz$. Figure 4-b shows the power confinement factor for TM modes (equation 39).

The power confinement factor of the TM modes decreases rapidly with frequency increase, but with slight effect of the core's radius. In either case the waveguide structure offers good guidance for both TE and TM modes over the specified frequency range and core's radii, but with preference to the TE modes and wider core's radius.

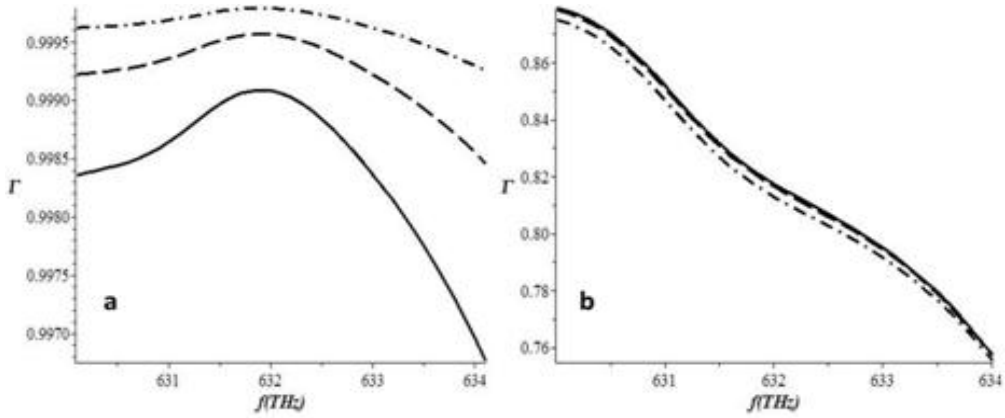

Figure 4: Power Confinement Factor for a. TE Mode, and b. TM Mode for Core's Radii a $= 4\mu m$ (Solid), $\mu m8$(Dashed), and $16\mu m$(Dot $-$ Dash) μm

In figure 5, we plotted the power attenuation (the imaginary part of equations (36 and 39)) versus frequency for different core's radii. In figure 5-a, the power attenuation for TE modes decreases with dielectric core radius increase, but for each core's radii the power attenuation increases with frequency increase. More power guidance leads to less power attenuation in the core, as it can be concluded from figure 4-a. In figure 5-b, the power attenuation for TM modes claims negative values, and have almost the same value for all dielectric core radii in use. The power attenuation for TM modes increases with frequency increase and flips back and decreases at almost $f = 632THz$. In general the TM modes suffer power attenuation more than the TE modes.

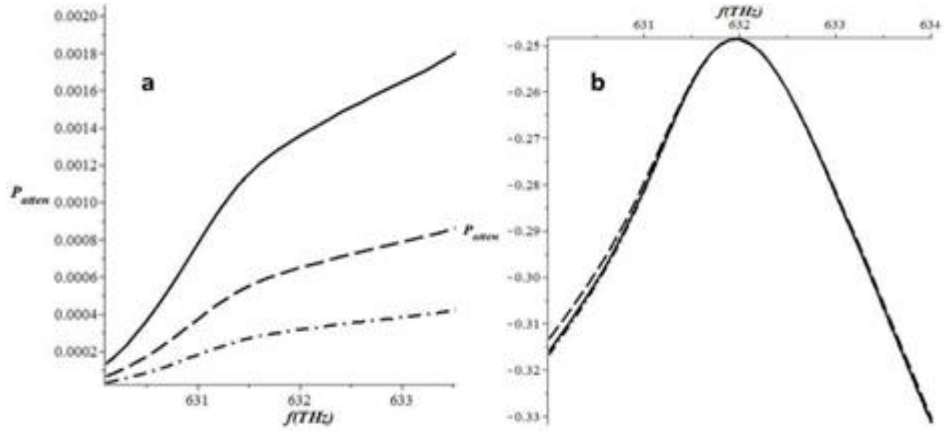

Figure 5: Power Attenuation for a. TE Mode, and b. TM Mode for Core's Radii $a = 4\mu m$(Solid), $\mu m8$(Dashed), and $16\mu m$(Dot $-$ Dash) μm

In figure 6, we use different class of Terahertz left handed material. In this material a closely-spaced pairs of gold nanorods are constructed for obtaining negative refractive index [29]. For this class of materials the real part of the refractive index becomes negative in the wavelength range from approximately $1400\ nm$ to $1600\ nm$, which includes the important telecommunication band at $1500\ nm = 200THz$. The effective refractive index [30-33] can be approximated to be $n_r = -0.3 \pm 0.1$and $\mu_{rn} = -1$.In figure 6, we plot the real part of the effective refractive index for TE mode.

The figure shows that structure offers law refractive index values in the allowed frequency spectrum. The core's thickness $a = 4\ \mu m$ exhibits the lowest value of real part of the effective refractive index, with positive slop, which means the waveguide structure behaves like right handed material with positive group velocity. The real part of the effective refractive index increases with both frequency and core's radius increase, but with different positive slopes.The waveguide structure does not support TM modes propagation.

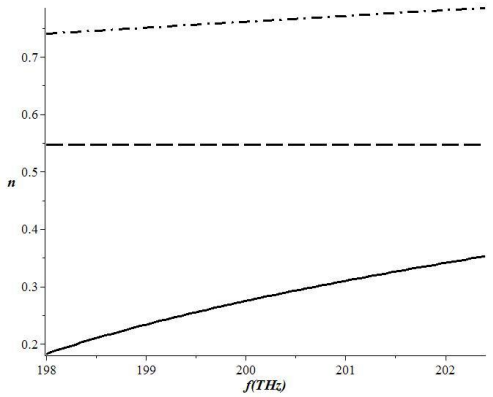

Figure 6: Real Part of the Effective Index Using Nanorods Metamaterial for TE Mode, and Core's Radii a = 4μm (Solid), μm8(Dashed), and 16μm(Dot − Dash) μm

In figure 7, we plot the power confinement factor for TE mode versus the allowed frequency range for different core's radii. Figure 7 shows that the power confinement factor has the highest value when the core radius $a = 16\mu m$, which means we have best power confinement at this core radius.

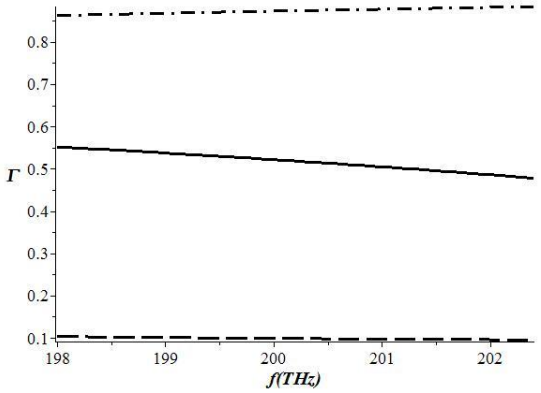

Figure 7: Power Confinement Factor Using Nanorods Metamaterial for TE Mode, and Core's Radii a = 4μm (Solid), μm8(Dashed), and 16μm(Dot − Dash) μm

CONCLUSIONS

We derived the TE and TM modal dispersion relation for cylindrical waveguide with dielectric core and Terahertz left-handed material. We have used two classes of left handed materials. The first class uses 3D nano-spheres distributed in loops in the dielectric host material, which gives rise to negative effective permeability and permeability between $630 \sim 634$ Terahertz. The second class is the nanorods which exhibits negative effective permeability and permeability at optical frequencies, between $198\ to\ 202\ THZ$, used in communications. Numerical solutionsfor the modal TE and TMdispersion relations showed that the waveguide structure exhibit low refractive index, low extinction coefficient, and high power confinement, which makes the structure a good candidate for many applications in communications. The core's radius $16\ \mu m$ resembles the best choice for power guidance through this waveguide structure.

REFERENCES

1. V. G. Veselago, "The electrodynamics of substances with simultaneously negative values of ε and μ," Soviet Physics Uspekhi, vol. 10, pp. 509–514, 1968,Uspekhi FizicheskikhNauk, vol. 92, pp. 517–526, 1967.
2. R. A. Shelby, D. R. Smith, and S. Schultz, "Experimental verification of a negative index of refraction," Science 292, 77–79, 2001.

3. C. Caloz and T. Itoh, “Application of the transmission line theory of lefthanded (LH) materials to the realization of a microstrip LH transmission line,” in Proc. IEEE-AP-S USNC/URSI National Radio Science Meeting, Vol. 2, San Antonio, June 2002

4. C. Caloz and T. Itoh, Electromagnetic Metamaterials: Transmission Line Theory and Microwave Applications, IEEE Press and Wiley, New York, 2005.

5. C. Caloz, and T. Itoh, “Transmission line approach of left-handed (LH) structures and microstrip realization of a low-loss broadband LH filter,” IEEE Trans. Antennas Propag., vol. 52, no. 5, pp. 1159–1166, May 2004.

6. C. Caloz and T. Itoh, “A novel mixed conventional microstrip and composite right/lefthanded backward-wave directional coupler with broadband and tight coupling characteristics,” IEEE Microwave Wireless Components Lett., vol. 14, no. 1, pp. 31–33, Jan. 2004

7. Sanshui Xiao, Linfang Shen, and Sailing He, “A Novel Directional Coupler Utilizing a Left-Handed Materia,” IEEE Photonic Technology Letters, VOL. 16, NO. 1, JANUARY 2004

8. Tingting Tang, , Wenli Liu, Xiujun He, Xiuying Gao, “A compact polarization splitter utilizing directional coupler with left-handed material,” Optik - International Journal for Light and Electron Optics Volume 123, Issue 12, June 2012

9. S. Otto, A. Rennings, C. Caloz, P. Waldow, I. Wolff, and T. Itoh, “Composite right/lefthanded λ-resonator ring antenna for dual-frequency operation,” in Proc. IEEE AP-S USNC/URSI National Radio Science Meeting, Washington, DC, June 2005.

10. Tingting Tang, “ Coarse wavelength division multiplexer–demultiplexer with left-handed material,” Optik - International Journal for Light and Electron Optics, 2013, inpress

11. Sanada, K. Murakami, I. Awai, H. Kubo, C. Caloz, and T. Itoh, “A planar zeroth order resonator antenna using a left-handed transmission line,” paper presented at 34th European Microwave Conference, Amsterdam, Netherlands, Oct. 2004.

12. I. I. Smolyaninov, Y. J. Hung and C. C. Davis, “Magni-fying Superlens in the Visible Frequency Range,” Science, Vol. 315, No. 5819, 2007, pp. 1699-1701. doi:10.1126/science.1138746

13. J. R. Tucker and M. J. Feldman, “Quantum Detection at Millimeter Wavelengths,” Review of Modern Physics, Vol. 57, No. 4, 1985, pp. 1055-1113. doi:10.1103/RevModPhys.57.1055

14. J. B. Pendry, A. J. Holden, W. J. Stewart, I. Youngs, “Extremely low frequency plasmons in metallic mesostructures.” Phys. Rev. Lett. 76, 4773-4776, 1996

15. H. T. Chen, W. J Padilla, J. M. O Zide, A. C. Gossard, A. J. Taylor, R. D. Averitt, “Active terahertz metamaterial devices.” Nature 444, 597-600, 2006

16. A. Alu, and A. Salandrino, “Negative effective permeability and lefthanded materials at optical frequencies,” Optics Express 14, 1557-1567, 2006.

17. Jie Yao, Zhaowei Liu, Yongmin Liu, Yuan Wang, Cheng Sun, Guy Bartal, Angelica M. Stacy, Xiang Zhang, “Optical Negative Refraction in Bulk Metamaterials of Nanowires,” Science, Vol 321, 2008

18. Andrea Vallecchi, and M. Albani, “Negative effective refractive index metamaterials at optical frequencies based

on superlattices of noble metals and excitonic semiconductors," General Assembly and Scientific Symposium, XXXth URSI. 10.1109/URSIGASS.2011.6050439, 2011

19. Changchun Yan, Dao Hua Zhang, Dongdong Li and Yuan ZhangDual, "refractions in metal nanorod-based Metamaterials," J. Opt. 12 065102 doi:10.1088/2040-8978/12/6/065102
20. S. Zhang, Fan W, Panoiu N C, Malloy K J, Osgood R M and Brueck S R J 2005 Experimental demonstration of near-infrared negative-index metamaterials Phys. Rev. Lett. 95 137404
21. J. D. Jackson, "Classical Electrodyanmics," John Wiley, 1998
22. M. J. Adams, "An Introduction to optical waveguides," John Wiley and Sons, 1981
23. Katsunari Okamoto, "Fundamentals of Optical Waveguides," Elsevier Inc, 2006
24. A. V. Novitsky andLMBarkovsky, "Guided modes in negative-refractive-index fibers," J. Opt. A: Pure Appl. Opt. 7 (2005)
25. Jai Singh, "Optical Properties of Condensed Matter and Applications," John Wiley, 2006
26. A. I. Ass'ad and H. S. Ashour, "TE Magnetostatic SurfaceWaves in Symmetric Dielectric Negative Permittivity Material Waveguide," Advances in Condensed Matter Physics, 2009
27. A. D. Boardman, M. M. Shabat, and R. F. Wallis, "TE waves at an interface between linear gyromagnetic and nonlinear dielectric media," Journal of Physics D, vol. 24, no. 10, pp. 1702–1707, 1991
28. Jörg Schilling, "The quest for zero refractive index, Fundamental optical physics," nature photonics, Vol 5, August 2011
29. Jiaming Hao, Wei Yan, and Min Qiu, "Super-reflection and Cloaking Based on Zero Index Metamaterial", Appl. Phys. Lett. 96, 101109 (2010)
30. Hsiao-Kuan Yuan, W. Cai, U. Chettiar, A. K. Sarychev, V. P. Drachev, A. V. Kildishev, V. M. Shalaev, "Optical Negative-Index Materials Based on Pairs of Metal Nanorods," OSA/FIO 2005
31. Vladimir M. Shalaev, Wenshan Cai, Uday K. Chettiar, Hsiao-Kuan Yuan, Andrey K. Sarychev,Vladimir P. Drachev, and Alexander V. Kildishev, "Negative index of refraction in optical metamaterials," OPTICS LETTERS / Vol. 30, No. 24 / December 15, 2005
32. Vladimir M. Shalaev, "Optical negative-index metamaterials," nature photonics, VOL 1, 2007
33. Thomas A. Klar, Alexander V. Kildishev, Vladimir P. Drachev, and Vladimir M. Shalaev, "Negative-Index Metamaterials: Going Optical," IEEE J. Selec. Top. Quant. Electron. 12, (2006).